**Accepted for publication in**

**Journal of Environmental Informatics**

# Reconstruction of snow water equivalent and snow depth using remote sensing data

**Quazi K. Hassan[1,*], Navdeep S. Sekhon[1], Robert Magai [2] and Preston McEachern[2]**

[1]Dept. of Geomatics Engineering, University of Calgary, 2500 University Drive NW, Calgary, Alberta, Canada T2N 1N4

[2] Science Innovation and Research Section, Clean energy Branch, Alberta Environment, Edmonton, Alberta, Canada T5G 1G4

*Corresponding author: E-Mail: qhassan@ucalgary.ca; Tel.: +1-403-210-9494; Fax: +1-403-284-1980.

**Abstract** Snow water equivalent (SWE) and snow depth are some of the most important quantities in describing the properties of the accumulated snow during winter, which is a source of runoff during spring season. Here, our objective was to reconstruct the spatial dynamics of SWE and snow depth over a study area in eastern parts of the northern Alberta during the period 2007-09. The employed methods consisted of: (i) delineating snow presence from MODIS-derived normalized difference snow index (NDSI)-images, (ii) calculating heating degree days (HDD) from MODIS-based surface temperature images, (iii) modelling net solar radiation, and (iv) integrating all of the above steps in the frame of a process based snow-melt model and SWE ground data as well. We used ~45% of the ground data (i.e., ~19 data points) in calibrating the values of base temperature and heating degree day coefficient for the model. Then the remaining ~55% of the ground data (i.e., 23 data points) were used in validation. It revealed that the agreement between the model and measured SWE-values were reasonable (i.e., 59%, 72%, and 62% of the time values were within ±20% deviations during 2007, 2008, and 2009 respectively). The root mean square deviation (RMSD) between the measured and modelled SWE-values were also reasonable and found to be ±24.75 mm in 2007, ±25.05 mm in 2008, and ±23.99 mm in 2009. Overall, the SWE-predictions at all of the measurement sites were on an average 7.5% higher in 2007, 10.2% lower in 2008, and 1.9% lower in 2009 than that of ground-based measurements. During the period 2007-2009, we found that the study area-specific average values of SWE and its depth were 177 mm and 694 mm respectively.

**Keywords:** MODIS; normalized difference snow index; heating degree days; net solar radiation; process based model; snow depth.

## 1. Introduction

Snow accumulation is a natural phenomenon over high latitudes (e.g., 50-70 $^{o}$N) during the winter months (Rodell and Houser, 2004; Bavera and Michele, 2009). One of the prime importances of snow accumulation is that it becomes a source of water supply in the watershed(s) during spring time (i.e., the usual snow melting period) (Cline et al., 1998; Maurer et al., 2003; Dozier and Painter, 2004; Durand and Margulis, 2007; Akyurek et al., 2010). In general, the snow accumulation (i.e., cover) can be described mainly using the properties of snow depth, equivalent water, and snow density (Fily et al., 1999; Ranzi et al., 1999; Dressler et al., 2006; Veatch et al., 2009; Kutchment et al., 2010). These properties may be measured precisely at point locations (e.g., Environment Canada's Weather Monitoring Stations, Alberta Environment Snow Monitoring Sites) (Bavera and Michele, 2009); however, it is unable to capture the spatio-temproal variability (Molotch and Margulis, 2008; Kutchment et al., 2010). Thus, in the scope of this study, we intend to develop methods in determining the properties of snow [i.e., snow water equivalent (SWE) and snow depth] at landscape scale.

In determining the snow depth, the most commonly employed method is the use of snow gauge. On the other hand, SWE can be determined using gravimetric method (i.e., collect a vertical core through the snowpack and then weighing or melting the core). The SWE can also be determined as a function of the snow depth and its density using the following expression (Bavera and Michele, 2009):

$$SWE = d_{SNOW}\left(\frac{\rho_{SNOW}}{\rho_{WATER}}\right) \quad (1)$$

where, $d_{SNOW}$ is the snow depth, $\rho_{SNOW}$ is the snow density, and $\rho_{WATER}$ is the density of water upon melting. Eq. 1 is normally used in determining the SWE at the locations, where the snow depth and its density are available usually at a gauge station (Bavera and Michele, 2009). These provide precise estimates at the point of measurements; however fail to delineate its dynamics at landscape level. To address this, it is possible to employ data interpolation techniques; but the outcome varies from technique to technique even using the same input dataset (Hassan et al., 2007a). Another alternate is the use of remote sensing-based methods, which has already been proven as a viable technique in snow related studies (Rodell et al., 2004; Bavera and Michele, 2009; Kutchment et al., 2010; Sekhon et al., 2010).

In most of the instances, the SWE mapping has been performed by incorporating optical remote sensing-based description of "% of snow cover area (SCA)" within a grid cell of interest (Rodell and Houser, 2004; Parajka and Bloschl, 2008; Bavera and Michele, 2009; Molotoch et al., 2009; Kuchment et al., 2010). The SCA can be delineated from normalized difference snow index [NDSI: a function of green (0.5-0.6 μm) and shortwave infrared (centred at 1.64 μm) spectral bands] derived from MODIS and LANDSAT satellite data (Rodell and Houser, 2004; Bavera and Michele, 2009; Molotoch et al., 2009). For example: (i) Rodell and Houser (2004) used MODIS-derived SCA in the framework of NASA's "Global Land Data Assimilation System" in modelling SWE at a minimum of 25 $km^2$ spatial resolution and 3 hourly temporal resolution covering the entire globe; (ii) Bavera and Michele (2009) incorporated MODIS-based SCA over Mallero basin in northern Italy; and (iii) Molotoch et al. (2009) employed both LANDSAT and MODIS-derived SCA in conjunction with a spatially distributed snow melt model, and implemented them over the southern Colorado mountain ranges in USA.

Upon delineating the temporal dynamics of the snow coverage, it can be possible to reconstruct SWE as a function of the energy available to melt the snow (Pietroniro and Leconte, 2005; Dressler et al., 2006; Molotch and Margulis, 2008; Hall et al., 2010). In the literature, the determination of such inflowing energy has been often calculated as a function of the heating degree days (HDD: an air temperature-based index) and net solar radiation (Brubaker et al., 1996; Melloh, 1999; Molotch and Margulis, 2008); which we would also like to adapt upon appropriate calibrations. In most of the instances, the maps of HDD have been derived from the interpolation of the measured air temperatures at the weather stations, which potentially may suffer from the spatial accuracy (Cline et al., 1998; Molotch and Margulis, 2008). The remote sensing data also have proven its effectiveness in developing temperature-related indices (e.g., Hassan et al, 2007a, b; Akther and Hassan, 2011), which might be useful in this context.

The overall objective of this study was to integrate remote sensing-based techniques and process-based models to reconstruct the landscape dynamics of SWE and snow depth at the onset of snow melting period during spring time in northern parts of Alberta, Canada (see Figure 1 for location information). The specific objectives were to:

i. develop relation among HDD, net solar radiation, and SWE during snow melting period at ground observation points;
ii. determine the timing of snow presence using NDSI temporal dynamics;
iii. reconstruct SWE maps at the onset of snow melting period during spring time from images of HDD and net solar radiation until snow presence using the relation developed in objective (i); and

iv. reconstruct snow depth as a function of SWE maps generated in objective (iii).

**Figure 1.**

## 2. Study area and data requirements

### *2.1. Study area*

The study area is 18312 $km^2$ lying in the eastern parts of northern Alberta as shown in the Figure 1 (shown as a rectangular box with dotted boundary). It falls within the Athabasca river basin, and geographically extends between 56.57- 57.95 $^{o}$N latitude and 110.41-112.37 $^{o}$W longitude. It is also part of four natural sub-regions (defined on the basis of vegetation, climate, topography, and soil type) in Alberta (Downing and Pettapiece, 2006); and details are shown in Figure 1b. A brief description of these natural sub-regions is also provided in Table 1.

In terms of major rivers, the Clearwater River is flowing from the east and merges into the Athabasca River in the south of the study area near Fort McMurray. The Athabasca River flows from southwest side of the province and goes towards north direction from Fort McMurray. In the context of topography, the average elevation of the study area is 435 metres above sea level ranging from 215 metres to 864 metres. The low lying areas are riparian Zone of Athabasca River and Clearwater River (see Figure 1c for more details).

**Table 1.**

### *2.2. Datasets used*

In this study, we acquired remote sensing data from MODIS (Moderate-resolution Imaging Spectroradiometer) and SWE measurement data from Alberta Environment. A brief description of these data is provided in Table 2.

**Table 2.**

## 3. Methodology

Figure 2 shows a schematic diagram of the method for reconstructing snow depth and snow water equivalent. It has following major compartments: (i) generation of HDD and net solar radiation as energy inputs; and (ii) comparing SWE with energy inputs until snow disappearance determined from NDSI temporal trends.

**Figure 2.**

Initially, the surface temperature and NDSI trends were extracted at the SWE measurement sites for the year of 2007-09. The temporal trends of NDSI were used to define the period of snow disappearance (i.e., when the values reached a minimum platform of negative values), which were found to have an overall accuracy of 93% (Hall and Riggs, 2007). It would be worthwhile to mention that there were some data gaps due to cloud contaminations in both $T_S$, and NDSI time-series, thus we excluded these pixels from further analysis. The average daily incident solar radiation at those locations was also modelled for the days of the snow-melt period using the solar radiation model described in Hassan et al. (2011) and enclosed in Appendix. In calculating

the incident solar radiation, the cloud cover information was required, which was obtained from Environment Canada (http://www.ec.gc.ca/) in the form of "% of possible daylight hours" (i.e., n/N in Eq. A.4). This particular model demonstrated strong relationships ($r^2$: 0.91-0.98) between ground-based measurements and modelled incident solar radiation at three test locations in Alberta (Hassan et al. 2011). From the incoming incident solar radiation, we computed the net solar radiation by making the following two assumptions: (i) the value of snow albedo to be 0.75, and (ii) value of net long wave radiations to be 30 W/m$^2$. We then employed the following equation in calculating SWE (Brubaker et al., 1996; Melloh, 1999):

$$SWE = a * \sum HDD + b * \sum R \quad (2)$$

$$HDD = \mathrm{T} - T_{base} \quad (3)$$

*where*, $a$ is the heating degree days coefficient; $T$ is the satellite-based temperature during the period of interest; $T_{base}$ is the base temperature (i.e., temperature above which snow melt is initiated); $b$ is the energy to water depth conversion ratio (0.026 cm W$^{-1}$ cm$^{-2}$ day$^{-1}$); and $R$ is the average net solar radiation during the periods of snow melt.

To determine the periods of snowmelt (i.e. the temporal window for summation of 'HDD' and 'R' in Eq. 2) we assumed the snowmelt to occur in the periods with temperature above $T_{base}$ until the period of snow disappearance (defined by NDSI temporal trend). In general, the base temperature of 273.15K is used in such studies of SWE modelling from air temperature (Molotch and Margulis, 2008). As this modeling was based on HDD computed from 'surface temperature' images, we performed a simultaneous investigation

into the value of $T_{base}$ around 273.15 K (i.e., in range of 270.15-274.15 K, at interval of 1 K).

Then, in order to determine the values of "*a*" in Eq. 2, we considered the SWE measurement sites within Athabasca river basin (i.e., 19 locations in 2007, 17 in 2008, and 19 in 2009; which were ~45% of the available data; see Figure 1 for location information). The remaining data were then used in validating the model (i.e., 21 locations in 2007, 25 in 2008, and 22 in 2009; which were ~55% of the available data). Note that the numbers of the ground measurement sites, both in the calibration and validation phases, were slightly different during the three years. It was due to the fact that some data points were declared outliers (4 in 2007, 2 in 2008, and 3 in 2009) in both of the calibration and validation phases. These outliers were chosen on basis of the ground observation values, regimes of surface temperature, and/or NDSI trends.

Finally, we used the validated model to estimate SWE in the study area during the years of 2007-09 from the images of surface temperature, NDSI, and net solar radiation. Then, snow depth map for each year was generated by multiplying the SWE map with the average snow density for that particular year of interest. The computation of average snow density for each year (using Eq. 1, and density of water at 4 °C) was from the set of simultaneous values for SWE and snow depth at the measurement sites during each year.

## 4. Results and discussion

Among the various evaluated base temperatures, the best agreements were found to be at $T_{base}$ of 272.15K. The base temperature of 272.15 K was appropriate; as the surface temperatures were instantaneous (that were acquired between 10:30am -12:30pm) and temperature regimes might increase during later in the noon that could largely contribute to the snow melting process.

Figures 3a, 4a, & 5a show the average trends of HDD accumulation (with a $T_{base}$ of 272.15 K), net solar radiation, and the averaged snow disappearance period; at all of the SWE measurement sites. It revealed that the snow disappeared during the 14$^{th}$ period (MODIS 8-day imaging epoch period, i.e. 3$^{rd}$ week of April) during each year of 2007-09. During the calibration phase for the year 2007 (see Figure 3b), we found that the value of "a" as 0.25 mm/°C/day provided the best agreements (i.e., within ±20% deviation for 68%). While during 2008, the results of calibration were similar (i.e., within ±20% deviation for 59%) for the values of "a" in the range 0.015 to 0.045 mm/°C day; we chose the value of 0.03 mm/°C day, which was in the middle. During 2009, we found that the agreements were similar (i.e., within ±20% deviation for ~60%) for the values of "a" in the range 0.3, 0.325, and 0.35 mm/°C day. However, on average of the deviations for all of the measurement sites results were best for 0.35 mm/°C/day (i.e. 5.6%, while for other two it was >8.5% lower of the ground measurements). Hence, we selected this as the "a" value for validation during 2009.

The variation in the values of "a" for the three years was due to the following factors: (i) inter-annual variability in the properties and dynamics of the snow accumulation (mainly of density and depth); and (ii) variability in the climatic conditions (cloudiness, temperature regimes, other

forms of precipitation), among others. However, the values of "a" for years of 2007 and 2009 were similar, but considerably different during the year of 2008. It might be associated to the significant differences in the amount of ground observed SWE during the 2008 (i.e., on an average 83 cm) from the other two years (i.e., on average 124 and 104 cm in 2007 and 2009 respectively). It would be interesting to note that the snow disappearance periods were similar among the years. Hence, the energy inflow computed from solar radiation in the three years was similar at different sites. Thus, the determination of a different value of the coefficient of "a" during 2008 (i.e., 0.03 mm/°C/day) in comparison to other two years would be reasonable.

**Figure 3.**

We then implemented the determined heating degree day coefficient "a" observed in Figures 3b, 4b & 5b at the remaining SWE measurement sites. It revealed that approximately 60% of the times the deviations between the modelled and measured SWE-values were within ±20% for all of the three years (see Table 3 for more detail information). We also determined the root mean square deviation (RMSD) between the measured and modelled SWE-values; and found to be ±24.75 mm in 2007, ±25.05 mm in 2008, and ±23.99 mm in 2009. In addition, we averaged all of the modelled SWE values and compared against that of the measured values at all of the ground locations. We found that the modelled-values of the SWE were 7.5% higher in 2007, 10.2% lower in 2008, and 1.9% lower in 2009.

**Figure 4.**

The deviations of the SWE estimates from the ground observed SWE might be associated to one of the following reasons: (i) uncertainties in the ground observations; (ii) atmospheric interactions in the remote sensing data; (iii) uncertainties posed by base temperature of 272.15 K; and (iv) difference in the scales of the phenomenon occurrence (dynamics of snow accumulation and melt, i.e. at instantaneous rate), its measurement (interval at which ground observations were made, i.e. 15 or 30 day interval), and its estimation (intervals at which remote sensing data was available, i.e. 8-days) (Rinne et al., 2009).

**Figure 5.**

**Table 3.**

The above described results (i.e., values of "a", base temperature, NDSI-images, surface temperature and solar radiation images) were used to reconstruct the spatial dynamics of SWE in the study area. However, we found that SWE in large portions of study area (greater than ~20%) had 'zero value'; and areas increased from 2007 to 2009. It was due to detection of a very early SDA period from the NDSI images. It might be due to interference caused to snow covers by the on-ground oil sand activity. Then we filled in these 'zero value' pixels by modeling SWE for all periods of positive NDSI (even after the early SDA) and AHDD (i.e. periods after attainment of 272.15K). Figure 6 shows example for both of the gap filled SWE and snow depth maps over the study area during 2008. The observed spatial variations in SWE and snow depth might be a function of variations in canopy type and coverage, slope and aspect, and wind speed; which were not in the scope of this paper.

**Figure 6.**

Note that the application of Eq. 1 revealed that the average density of the snow at measurement sites was 0.23 gm/cm$^3$ for 2007 and 2009, while 0.21 gm/cm$^3$ for 2008; and used to generate the snow depth maps as a function of SWE maps. During the years of 2007-2009, we found that the study area-specific average values of SWE and its depth were 148 mm and 667 mm respectively. In general, the accumulation of SWE was higher towards northern latitudes and higher elevation areas. The elevation and slope were having larger effect on snow accumulation than the latitude. Also, the SWE was very low for the slopes of elevated areas and towards the riparian zone; which might be associated with vegetation coverage.

## 5. Concluding remarks

In this study, we demonstrated the potential of reconstructing SWE and depth of the snow covers by integrating MODIS-based observations (i.e., HDD and NDSI), ground observations (i.e. SWE measures), and modelling of net solar radiation; in the northern part of Alberta. We explored the implementation of energy-inflow based snowmelt modeling method in this study, with an appropriate calibration and validation phases during the years of 2007-09. We found reasonable agreements (i.e., within ±20% of the ground measured value for ~60% of the cases) between the estimated values and the ground-based measurements of the SWE. Then this calibrated and validated model was used to obtain comprehensive maps of SWE for the study area. The application of the methods as described here establishes the potential of such techniques in reconstruction of the SWE at landscape scales.

**Acknowledgments**

This study was funded by Alberta Environment under a research contract to Q. K. Hassan. The authors would also like to acknowledge (i) NASA for freely providing MODIS data; and (ii) Alberta Environment for providing ground data.

**References**

Akyurek, Z., Hall, D.K., Riggs, G.A., Sensoy, A., 2010. Evaluating the utility of the ANSA blended snow cover product in the mountains of eastern Turkey. International Journal of Remote Sensing 31, 3727-3744.

Bavera, D., Michele, C.D., 2009. Snow water equivalent estimation in the Mallero basin using snow gauge data and MODIS images and fieldwork validation. Hydrological Processes 23, 1961-1972.

Brubaker, K., Rango, A., Kustas, W., 1996. Incorporating radiation inputs into the snowmelt runoff model. Hydrological Processes 10, 1329-1343.

Cline, D.W., Bales, R.C., Dozier, J., 1998. Estimating the spatial distribution of snow in mountain basins using remote sensing and energy balance modeling. Water Resources Research 34, 1275-1285.

Downing, D.J., Pettapiece, W.W. (Eds.), 2006. *Natural Regions and Subregions of Alberta*;; Pub. No. T/852; Natural Regions Committee: Government of Alberta, Alberta, Canada.

Dozier, J., Painter, T.H., 2004. Multispectral and hyperspectral remote sensing of Alpine snow properties. Annual Reviews Earth Planet Science 32, 465-494.

Dressler, K.A., Leavesley, G.H., Bales, R.C., Fassnacht, S.R., 2006. Evaluation of gridded snow water equivalent and satellite snow cover products for mountain basins in a hydrologic model. Hydrological Processes 20, 673-688.

Durand, M., Margulis, S.A., 2007. Correcting first-order errors in snow water equivalent estimates using a multifrequency, multiscale radiometric data assimilation scheme. Journal of Geophysical Research 112, D13121.

Fily, M., Dedieu, J.P., Durand, Y., 1999. Comparison between the results of a snow metamorphism model and remote sensing derived snow parameters in the Alps. Remote Sensing of Environment 68, 254-263.

Hall, D.K., and Riggs, G.A., 2007. Accuracy assessment of the MODIS snow products. Hydrological Processes 21, 1534-1547.

Hassan, Q.K., Bourque, C.P.-A., Meng, F.R., Richards, W., 2007a. Spatial mapping of growing degree days: an application of MODIS-based surface temperatures and enhanced vegetation index. Journal of Applied Remote Sensing 1, 013511:1-013511:12.

Hassan, Q.K., Bourque, C.P.-A., Meng, F.R., 2007b. Application of Landsat-7 ETM+ and MODIS products in mapping seasonal accumulation of growing degree days at enhanced resolution. Journal of Applied Remote Sensing 1, 013539:1-013539:10.

Hassan, Q.K., Rahman, K.M., Haque, A.S., Ali, A., 2011. Solar energy modelling over a residential community in the City of Calgary, Alberta, Canada. International Journal of Photoenergy 216519:1-216519:8.

Kutchment, L.S., Romanov, P., Gelfan, A.N., Demidov, V.N., 2010. Use of satellite-derived data for characterization of snow cover and simulation of snowmelt runoff through a distributed

physically based model of runoff generation. Hydrology and Earth System Sciences 14, 339-350.

Maurer, E.P., Rhoads, J.D., Dubayah, R.O., Lettenmaier, D.P., 2003. Evaluation of the snow-covered area data product from MODIS. Hydrological Processes 17, 59-71.

Melloh, R.A., 1999. A synopsis and comparison of selected snowmelt algorithms. Cold Regions Research & Engineering Laboratory (CRREL) technical publication.

Molotch, N.P., Brooks, P.D., Burns, S.P., Litvak, M., Monson, R.K., McConnell, J.R., Musselman, K., 2009. Ecohydrological controls on snowmelt partitioning in mixed-conifer sub-alpine forests. Ecohydrology 2, 129-142.

Molotch, N.P., Margulis, S.A., 2008. Estimating the distribution of snow water equivalent using remotely sensed snow cover data and a spatially distributed snowmelt model: A multi-resolution, multi-sensor comparison. Advances in Water Resources 31, 1503-1514.

Parajka, J., Bloschl, G., 2008. The value of MODIS snow cover data in validating and calibrating conceptual hydrologic models. Journal of Hydrology 358, 240– 258.

Pietroniro, A., Leconte, R., 2005. A review of Canadian remote sensing and hydrology, 1999-2003. Hydrological Processes 19, 285-301.

Ranzi, R., Grossi, G., Bacchi, B., 1999. Ten years of monitoring areal snowpack in the Southern Alps using NOAA-AVHRR imagery, ground measurements and hydrological data. Hydrological Processes 13, 2079-2095.

Rinne, J., Aurela, M., Manninen T., 2009. A Simple Method to Determine the Timing of Snow Melt by Remote Sensing with Application to the $CO_2$ Balances of Northern Mire and Heath Ecosystems. Remote Sensing 1, 1097-1107.

Rodell, M., Houser, P.R., 2004. Updating a land surface model with MODIS-derived snow cover. Journal of Hydrometeorology 5, 1064-1075.

Rodell, M., Houser, P.R., Jambor, U., Gottschalck, J., Mitchell, K., Meng, C.-J., Arsenault, K., Cosgrove, B., Radakovich, J., Bosilovich, M., Entin, J.K., Walker, J.P., Lohmann, D., Toll, D., 2004. The Global Land Data Assimilation System, Bulletin of American. Meteorological Society 85, 381-394.

Sekhon, N.S., Hassan, Q.K., Sleep, R.W., 2010. Evaluating potential of MODIS-based indices in determining "Snow Gone" stage over forest-dominant regions. Remote Sensing 2, 1348-1363.

Veatch, W., Brooks, P.D., Gustafson, J.R., Molotch, N.P., 2009. Quantifying the effects of forest canopy cover on net snow accumulation at a continental, mid-latitude site. Ecohydrology 2, 115-128.

Zhang, Y., Yan, S., Lu, Y., 2010. Snow Cover Monitoring Using MODIS Data in Liaoning Province, Northeastern China. Remote Sensing 2, 777-793.

## Appendix

*Equations for modelling of the average incident solar radiation*

In calculating the daily net solar radiation on a horizontal plane at a location of SWE reconstruction, we used the following equations:

$$R_{net} = \left(R_{SW}^{in} - R_{SW}^{out}\right) + \left(R_{LW}^{in} - R_{LW}^{out}\right) \quad \text{(A.1)}$$

$$R_{SW}^{out} = \alpha * R_{SW}^{in} \quad \text{(A.2)}$$

$$\left(R_{LW}^{in} - R_{LW}^{out}\right) \approx 30 \ W.m^{-2} \quad \text{(A.3)}$$

$$R_{SW}^{in} = \left(a + b\frac{n}{N}\right) * R_{daily-ex} \quad \text{(A.4)}$$

$$R_{daily-ex} = \frac{1}{\pi} E_0 d_r \left[\omega_s \sin(\phi)\sin(\delta) + \cos(\phi)\cos(\delta)\sin(\omega_s)\right] \quad \text{(A.5)}$$

$$d_r = 1 + 0.033\cos\left(\frac{2\pi}{365} DOY\right) \quad \text{(A.6)}$$

$$\delta = 0.409\sin\left(\frac{2\pi}{365} DOY - 1.39\right) \quad \text{(A.7)}$$

$$Radians = \frac{\pi}{180}[\text{decimal degrees}] \quad \text{(A.8)}$$

$$\omega_s = \arccos[-\tan(\phi)\tan(\delta)] \quad \text{(A.9)}$$

where,

$R_{net}$ is the daily net solar radiation [W.m$^{-2}$];

$R_{SW}^{in}$ is the daily incoming shortwave solar radiation [W.m$^{-2}$];

$R_{SW}^{out}$ is the daily outgoing shortwave solar radiation [W.m$^{-2}$];

$R_{LW}^{in}$ is the daily incoming longwave solar radiation [W.m$^{-2}$];

$R_{LW}^{out}$ is the daily outgoing longwave radiation [W.m$^{-2}$];

$\alpha$ is the surface albedo (~0.75 for snow cover);

$R_{daily\text{-}ex}$ is the daily extra-terrestrial radiation [W.m$^{-2}$];

$a$ (=0.25) is an Angstrom value [dimensionless];

$b$ (=0.50) is an Angstrom value [dimensionless];

$n/N$ is the % of possible daylight hours (i.e., form of bright sunshine hours) [dimensionless];

$E_0$ is the solar constant = 1353 W.m$^{-2}$;

$d_r$ is the inverse relative distance between earth-sun; $\delta$ is the solar declination angle [radians];

$\phi$ is the latitude [radians];

$\omega_s$ is the sunset hour angle [radians]; and

$DOY$ is the number of the day in the year between 1 (1 January) and 365 or 366 (31 December).

## ***List of Tables***

**Table 1.** Brief description of the 4 natural subregions within study area (modified after Downing and Pettapiece (2006)).

| Natural sub-region | Area in each sub-region ($km^2$) | Mean annual Temp. ( °C) | Mean annual precip. (mm) | Dominant vegetation |
|---|---|---|---|---|
| **Central Mixedwood** | 13762 | 0.2 | 478 | Deciduous, mixedwood |
| **Lower Boreal Highlands** | 864 | −1.0 | 495 | Early to mid-seral pure or mixed forests hybrids |
| **Upper Boreal Highlands** | 1368 | −1.5 | 535 | Conifer dominated |
| **Athabasca Plain** | 2318 | −1.2 | 428 | Conifers (*Pinus*), dunes largely unvegetated |

**Table 2.** Brief description of the required data in this study.

| Source | Data type | Description |
|---|---|---|
| NASA | MODIS-based 8-day surface temperature at 1km spatial resolution (i.e., MOD11A2). | These were used to calculate the heating degree days (HDD). |
| NASA | MODIS-derived 8-day normalized difference snow index (NDSI)-images at 500m spatial resolution were acquired. Those were derived from MODIS-based surface reflectance product (i.e., MOD09A1 v.005) as a function of surface reflectance from green and short wave infrared (SWIR centered at 2.13µm) spectral bands. | These were used to define the snow disappearance period during the spring season |
| Alberta Environment | Snow depth and snow water equivalent data at point measurement sites. | These were used to determine snow equivalent water, which then be used to establish relation with inflowing energy. |

**Table 3.** The validation results as % of the ground measurement sites for the values of % observed deviation, where 'n' is number of sites, and 'a' is heating degree day coefficient

| *Year* | *n* | *a* | *Deviation (%)* | | | | | | | |
|---|---|---|---|---|---|---|---|---|---|---|
| | | | **± 5** | **± 10** | **± 15** | **± 20** | **± 25** | **± 30** | **± 35** | **≥ ± 40** |
| **2007** | *21* | **0.25** | 23 | 36 | 45 | 59 | 77 | 91 | 95 | 100 |
| **2008** | *25* | **0.03** | 16 | 32 | 48 | 72 | 80 | 84 | 84 | 100 |
| **2009** | *22* | **0.35** | 10 | 24 | 38 | 62 | 76 | 81 | 81 | 100 |

## ***List of Figures***

**Figure 1.** Description of the study area, with **(a)** location of the study area in Alberta shown using rectangular dotted box, and the black dots are showing the Alberta Environment station sites from where SWE and snow depth measurement records were acquired; **(b)** spatial extent of the four natural sub-regions within the study area; and **(c)** major river networks along with the elevation information.

**Figure 2.** Schematic diagram of the methods employed in logical modeling of SWE.

**Figure 3. (a)** The averaged trends of accumulated HDD, net solar radiation (R); and the average snow disappearance (SDA) period on the basis of NDSI-values during 2007; **(b)** calibration of heating degree days coefficient "*a*" using the SWE measurements at all of the 19 sites within Athabasca river basin during 2007.

**Figure 4. (a)** The averaged trends of accumulated HDD, net solar radiation (R); and the average snow disappearance (SDA) period on the basis of NDSI-values during 2007; **(b)** calibration of heating degree days coefficient "*a*" using the SWE measurements at all of the 19 sites within Athabasca river basin during 2008.

**Figure 5. (a)** The averaged trends of accumulated HDD, net solar radiation (R); and the average snow disappearance (SDA) period on the basis of NDSI-values during 2007; **(b)** calibration of heating degree days coefficient "*a*" using the SWE measurements at all of the 19 sites within Athabasca river basin during 2009.

**Figure 6.** Spatial dynamics and areal distribution for: **(a)** SWE during 2008; and **(b)** snow depth during 2008.

**Figure 1.**

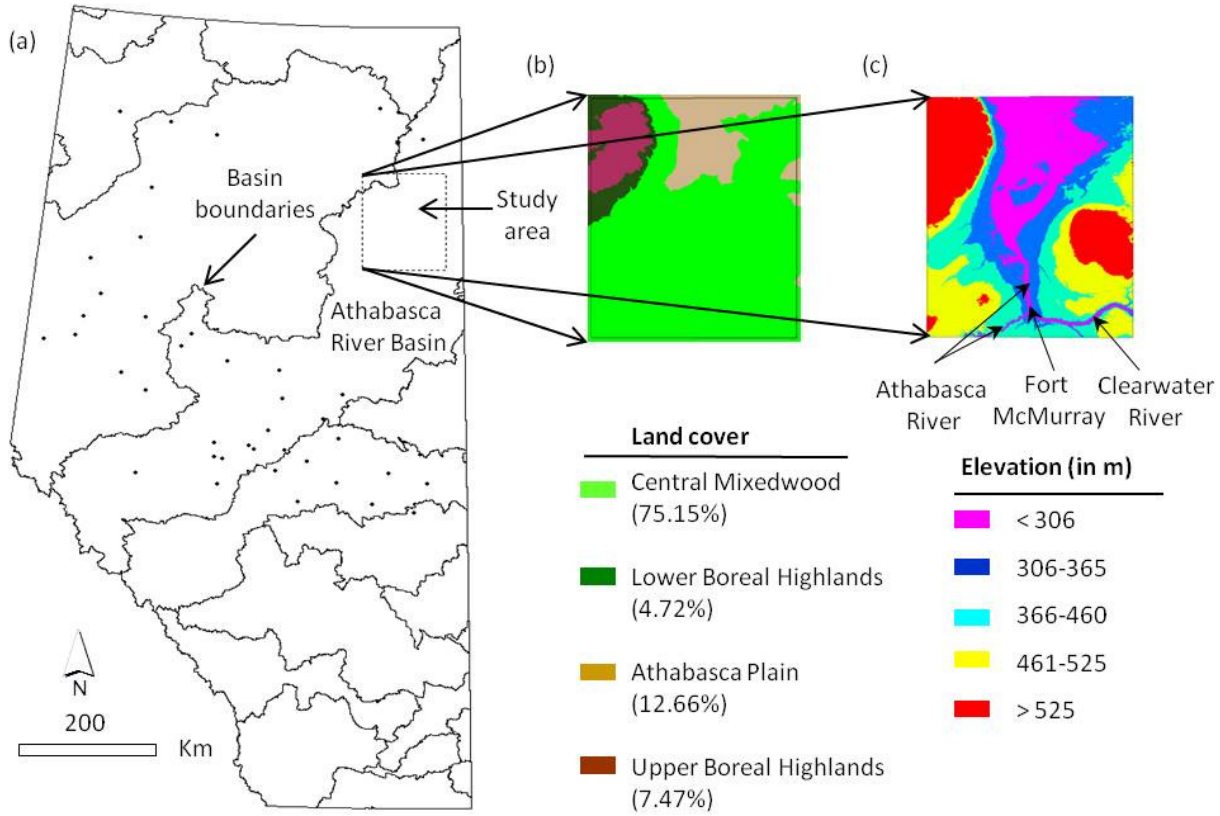
(a)
(b)
(c)
Basin boundaries
Study area
Athabasca River Basin
N
200
Km
Athabasca River
Fort McMurray
Clearwater River
Land cover
Central Mixedwood (75.15%)
Lower Boreal Highlands (4.72%)
Athabasca Plain (12.66%)
Upper Boreal Highlands (7.47%)
Elevation (in m)
< 306
306-365
366-460
461-525
> 525

**Figure 2.**

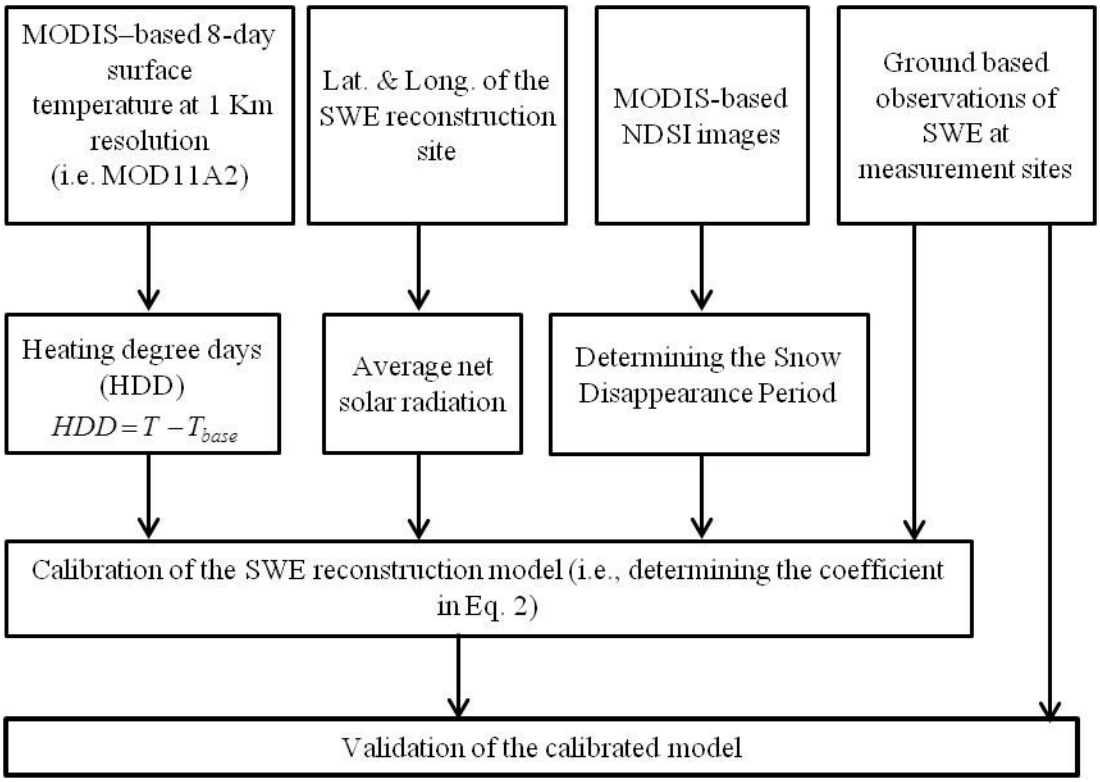
MODIS–based 8-day surface temperature at 1 Km resolution (i.e. MOD11A2)
Lat. & Long. of the SWE reconstruction site
MODIS-based NDSI images
Ground based observations of SWE at measurement sites
Heating degree days (HDD)
$HDD = T - T_{base}$
Average net solar radiation
Determining the Snow Disappearance Period
Calibration of the SWE reconstruction model (i.e., determining the coefficient in Eq. 2)
Validation of the calibrated model

**Figure 3.**

(a)

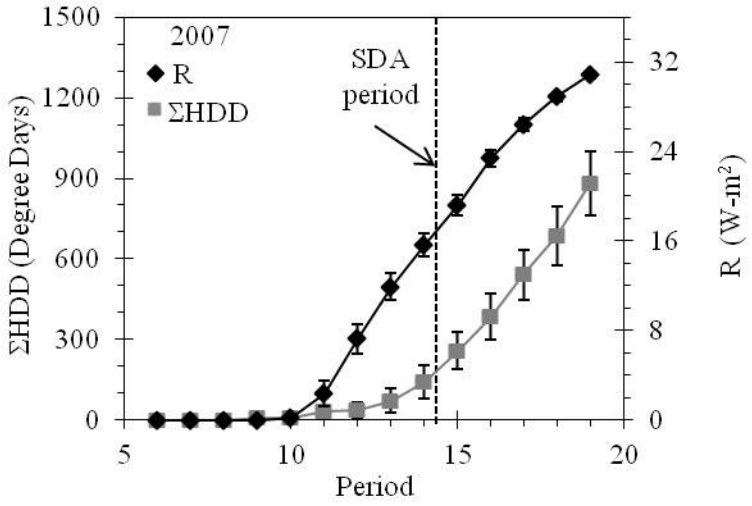


(b)

| *% of 19 SWE measurement sites* | | | | | | | |
|---|---|---|---|---|---|---|---|
| *Devia-* | *Heating Degree Day Coefficient* | | | | | | |
| *tion* | **0.175** | **0.2** | **0.225** | **0.25** | **0.275** | **0.3** | **0.325** |
| ± **5** | 5 | 21 | 21 | 26 | 26 | 32 | 26 |
| ± **10** | 26 | 37 | 42 | 47 | 53 | 53 | 42 |
| ± **15** | 53 | 47 | 63 | 68 | 68 | 58 | 58 |
| ± **20** | 63 | 79 | 79 | 68 | 68 | 74 | 68 |
| ± **25** | 79 | 79 | 79 | 84 | 79 | 74 | 68 |
| ± **30** | 84 | 84 | 84 | 84 | 84 | 84 | 74 |
| ± **35** | 84 | 84 | 84 | 84 | 84 | 84 | 84 |
| ≥ ± **40** | 100 | 100 | 100 | 100 | 100 | 100 | 100 |

**Figure 4.**

(a)

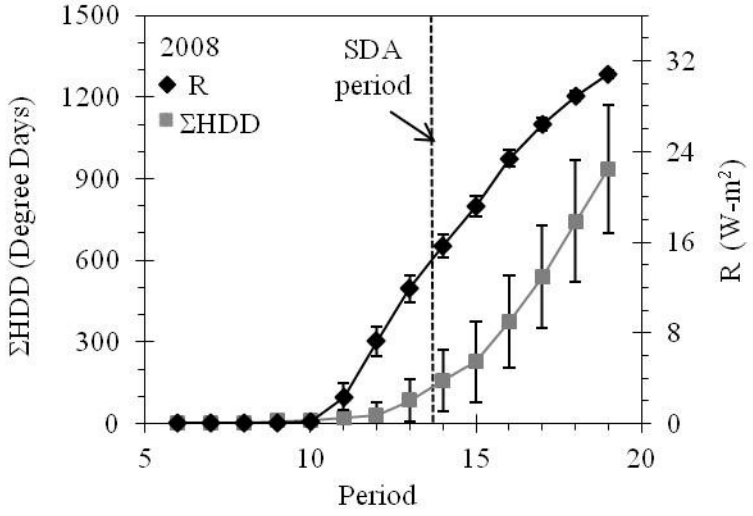


(b)

| *% of 17 SWE measurement sites* | | | | | | | |
|---|---|---|---|---|---|---|---|
| *Deviation* | *Heating Degree Day Coefficient* | | | | | | |
| | **0.015** | **0.02** | **0.025** | **0.03** | **0.035** | **0.04** | **0.045** |
| ± **5** | 24 | 24 | 24 | 12 | 12 | 6 | 12 |
| ± **10** | 35 | 29 | 24 | 24 | 29 | 29 | 35 |
| ± **15** | 41 | 41 | 47 | 47 | 53 | 53 | 53 |
| ± **20** | 59 | 59 | 59 | 59 | 59 | 59 | 59 |
| ± **25** | 59 | 59 | 59 | 59 | 59 | 59 | 59 |
| ± **30** | 65 | 65 | 65 | 65 | 65 | 65 | 65 |
| ± **35** | 65 | 65 | 65 | 65 | 65 | 65 | 65 |
| ≥± **40** | 100 | 100 | 100 | 100 | 100 | 100 | 100 |

**Figure 5.**

(a)

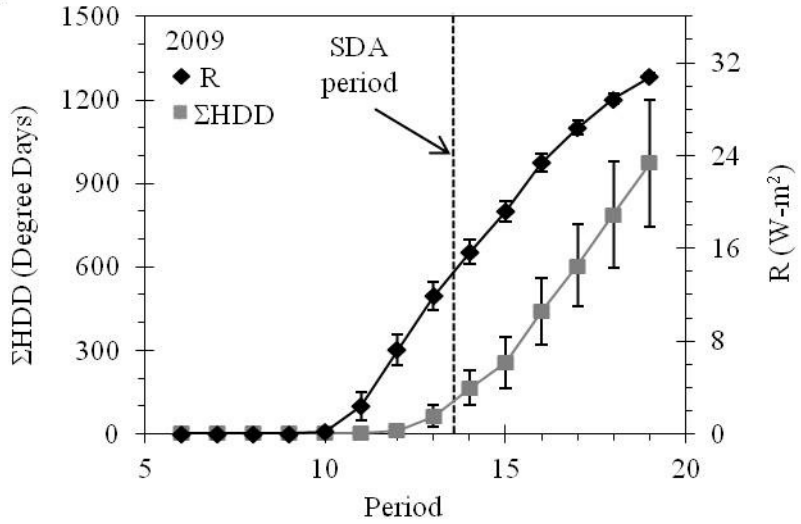


(b)

| *% of 19 SWE measurement sites* | | | | | | | |
|---|---|---|---|---|---|---|---|
| *Deviation* | *Heating Degree Day Coefficient* | | | | | | |
| | **0.25** | **0.275** | **0.3** | **0.325** | **0.35** | **0.375** | **0.4** |
| **± 5** | 26 | 26 | 37 | 21 | 16 | 16 | 5 |
| **± 10** | 47 | 53 | 42 | 47 | 37 | 26 | 21 |
| **± 15** | 53 | 58 | 58 | 53 | 53 | 47 | 37 |
| **± 20** | 58 | 58 | 63 | 63 | 58 | 58 | 53 |
| **± 25** | 68 | 68 | 63 | 68 | 68 | 68 | 58 |
| **± 30** | 68 | 74 | 74 | 68 | 74 | 74 | 74 |
| **± 35** | 74 | 74 | 79 | 79 | 79 | 79 | 84 |
| **≥ ± 40** | 100 | 100 | 100 | 100 | 100 | 100 | 100 |

**Figure 6.**

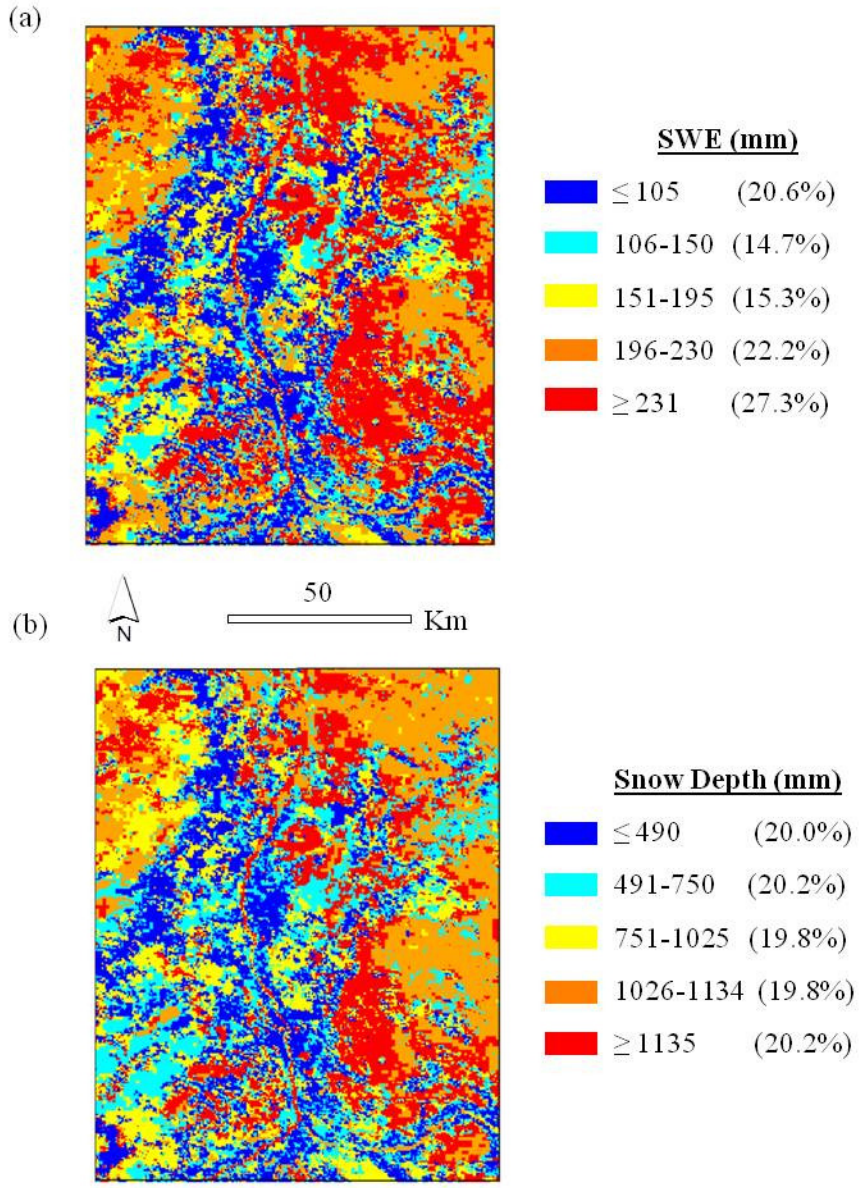
(a)
SWE (mm)
≤105 (20.6%)
106-150 (14.7%)
151-195 (15.3%)
196-230 (22.2%)
≥231 (27.3%)
(b)
N
50
Km
Snow Depth (mm)
≤490 (20.0%)
491-750 (20.2%)
751-1025 (19.8%)
1026-1134 (19.8%)
≥1135 (20.2%)